Available online at www.sciencedirect.com
ScienceDirect
Geochimica et Cosmochimica Acta 74 (2010) 3851–3862
Geochimica et Cosmochimica Acta
www.elsevier.com/locate/gca

Ruthenium endemic isotope effects in chondrites and differentiated meteorites

J.H. Chen [a,*], D.A. Papanastassiou [a,b], G.J. Wasserburg [b]

[a] *Science Division, Jet Propulsion Laboratory, M/S 183-601, California Institute of Technology, 4800 Oak Grove Drive, Pasadena, CA 91109, USA*

[b] *Division of Geological and Planetary Sciences, M/C 170-25, 1200 E. California Blvd., California Institute of Technology, Pasadena, CA 91125, USA*

Received 18 May 2009; accepted in revised form 7 April 2010; available online 21 April 2010

Abstract

We report on the abundances of Ru isotopes in (1) iron meteorites, (2) stony-iron meteorites (pallasites), (3) ordinary and carbonaceous chondrites, and (4) in refractory inclusions from the carbonaceous meteorite Allende. We have developed improved Multiple-Collector, Negative-ion Thermal Ionization Mass Spectrometric (MC-NTIMS) techniques for Ru, with high ionization efficiency of 4% and with chemical separation techniques for Ru, which reduce mass interferences to the ppm level, so that no mass interference corrections needed to be applied. Our data were normalized to $^{99}Ru/^{101}Ru$ to correct for mass-dependent fractionation. We find no Ru isotopic effects in the ordinary chondrites and group IAB iron meteorites we have measured. There are significant effects (deficits) in the pure s-process nuclide ^{100}Ru, in the Allende whole-rock and in refractory inclusions of up to 1.7 parts in 10,000 (εu). There are also endemic deficits in ^{100}Ru in iron meteorites and in pallasites of up to 1.1 εu. The Ru data suggest a wide spread and large scale heterogeneity in p-, s-, and r-process components resulting in a deficit in s-process nuclides or enhancements in both p- and r-process nuclides, in refractory siderophiles condensing in the early solar nebula. In contrast, the data on bulk Murchison suggest an excess in ^{100}Ru and in ^{104}Ru, which are distinct from the rest of the measured patterns. Our results establish the presence of significant isotopic heterogeneity for Ru in the early solar nebula. The observation of endemic Ru effects in planetary differentiates, such as iron meteorites and pallasites, must reflect the siderophile nature of Ru and the preservation in condensing FeNi metal of refractory metal condensate grains formed in the early solar nebula. Once incorporated in the metal phase, the refractory siderophiles remained in the metal phase through the melting and differentiation of planetesimals to form FeNi cores and silicate mantles and crusts.

1. INTRODUCTION

We report on the abundances of Ru isotopes in iron meteorites, stony-iron meteorites (pallasites), ordinary and carbonaceous chondrites, and in refractory inclusions in the carbonaceous meteorite Allende. The abundances of short-lived p-, s-, and r-nuclides in the interstellar medium at the beginning of the solar system can be derived from modeling of galactic chemical evolution and stellar nucleosynthesis. They can also be determined from measurements of solar system materials in the laboratory. Comparison between the theoretical and observed abundances provides further insight into the origin of extinct radionuclides and processes in the early solar system. Recent measurements on unequilibrated chondritic meteorites provide high precision isotopic data for the ratios between slow neutron-capture process (s-process) and rapid neutron-capture process (r-process) isotopes for heavy elements. These data are useful to test the theoretical predictions for the s-process in the He-burning shell of AGB stars or r-process in supernovae (Wasserburg et al., 1994, 1996; Barzyk et al., 2007; Reisberg et al., 2009). Isotopic anomalies were reported in bulk

* Corresponding author. Tel.: +1 8183549381.
E-mail address: james.h.chen@jpl.nasa.gov (J.H. Chen).

0016-7037/$ - see front matter © 2010 Elsevier Ltd. All rights reserved.
doi:10.1016/j.gca.2010.04.013

carbonaceous chondrites for Sr, Mo, Ba, Sm, Nd, and Os (e.g., Dauphas et al., 2002; Yin et al., 2002; Brandon et al., 2005; Ranen and Jacobsen, 2006; Andreasen and Sharma, 2006, 2007; Carlson et al., 2007). In contrast, the isotopic compositions of Te, Zr, Mo, Ru, and Os in bulk carbonaceous meteorites were reported to be isotopically identical to terrestrial values (Becker and Walker, 2003a,b; Schönbächler et al., 2005; Fehr et al., 2006; Yokoyama et al., 2007). Stepwise dissolutions of the carbonaceous chondrites Orgueil (CI), Murchison (CM), and Allende (CV) reveal large nucleosynthetic anomalies for Zr isotopes that contrast with the uniform compositions found in bulk meteorites (Schönbächler et al., 2005). Similarly, acid insoluble residues of three carbonaceous chondrites are enriched in s-process Os isotopes while depleted in acid soluble portions of the same meteorites (Reisberg et al., 2007, 2009; Yokoyama et al., 2007). These anomalies in carbonaceous chondrites were interpreted either in terms of an inhomogeneous distribution within the solar nebula or in terms of the selective dissolution of pre-solar grains that carried large isotope anomalies. Individual isotopic analyses of pre-solar grains for Sr, Zr, Mo, Ru, Ba, Hf, and some rare earth elements are available (e.g., Nicolussi et al., 1998a,b,c; Davis et al., 2001; Lugaro et al., 2003; Savina et al., 2003, 2004; Yin et al., 2006; Barzyk et al., 2006, 2007; Marhas et al., 2007).

Precise isotopic determinations of heavy elements such as Ru could provide some clues to their origin. Ru has two p-only (^{96}Ru, ^{98}Ru), one s-only (^{100}Ru), one r-only (^{104}Ru) and three mixed s- and r-process isotopes (^{99}Ru, ^{101}Ru, and ^{102}Ru). The p-process isotopes of Ru show large abundances (5.5% and 1.9%) relative to typically low p-process isotope abundances, at the permil level, for most elements. These large abundances of p-process isotopes have been hard to explain through the standard nucleosynthetic processes. Preserved effects from incomplete mixing of Ru components from different nucleosynthetic sources would yield general isotope anomalies in Ru. Ru isotopes could also show effects in ^{98}Ru and ^{99}Ru from the decay of short-lived ^{98}Tc and ^{99}Tc, in the early solar system. The prior presence of these extinct radionuclides could be inferred from the excesses or deficits of their daughter nuclides among different objects in the solar system. The half-life of ^{98}Tc is poorly constrained ($t_{½} = 4.2$–10 Ma, Kobayashi et al., 1993; Firestone and Shirley, 1996). The half-life of ^{99}Tc is only 0.21 Ma (Firestone and Shirley, 1996). The short half-life of ^{99}Tc implies that any enrichment of ^{99}Ru in early solar system objects would include very early and efficient Tc–Ru chemical fractionation. It would provide additional constraints on the decay interval between the formation of s-process nuclides and incorporation into objects in the solar nebula (e.g., Wasserburg, 1985). In addition, the ^{98}Tc–^{98}Ru decay system, with the longer half-life, comparable to the half-lives for the ^{53}Mn–^{53}Cr ($t_{½} = 3.7$ Ma), ^{107}Pd–^{107}Ag ($t_{½} = 6.5$ Ma) and ^{182}Hf–^{182}W ($t_{½} = 9$ Ma) systems, may yield important information about the history of the early solar system and place precise constraints on the relative time scales of these processes (Lugmair and Galer, 1992; Nyquist et al., 1994; Lee and Halliday, 1995, 2000; Chen and Wasserburg, 1996). However, ^{98}Tc is an odd-odd nuclide, whose production would be expected to be low.

Both radiogenic and general isotope anomalies are important in understanding the processes for the formation of the early solar system. The current emphasis on Ru is predicated on the development of Negative-ion Thermal Ionization Mass Spectrometry (NTIMS) and of Multiple Collector Inductively Coupled Mass Spectrometry (MC-ICP-MS). For this work, we have developed techniques for the clean chemical separation of Ru and for isotope measurements using MC-NTIMS.

2. ANALYTICAL PROCEDURES

2.1. Samples and sample preparation

We analyzed whole-rock samples from six chondrites (Olivenza, Portales Valley, Ransom, Garnet, Murchison, and Allende). Metal-rich material from Olivenza was also separated using a hand magnet. In addition, we analyzed four Allende Ca–Al-rich Inclusions (CAI, type B, coarse-grained: Egg 3, Egg 6, and BigAl; and fine-grained: Pink Angel). We sampled FeNi metal from fourteen iron meteorites of different chemical groups, including four non-magmatic irons (IAB, Canyon Diablo and Pitts; IVB, Hoba and Tlacotepec), nine magmatic irons (IIAB, Bennett County, Negrillos, Coahuila; IIIAB, Cape York, Grant, Acuna, Bella Roca, Tres Castillos; IVA, Gibeon), and one ungrouped iron (Piñon). In addition, we analyzed metal samples from three pallasites (Salta, Springwater, and Thiel Mountain). Metal cubes, weighing about 100–500 mg, were cut from the individual meteorite slabs and inspected to be free from any inclusions or rust. The cubes were etched with hot aqua regia (2:1, conc. HCl/conc. HNO_3) and then HCl, to remove a thin surface layer. All "whole-rock" chondrite samples were taken from powders prepared previously. The fragments of the Allende CAI were also prepared previously. If multiple samples were taken from the same meteorite for analyses, we labeled them as "−1", "−2". In this study, all duplicate samples were taken from the same metal slab. We labeled duplicate analyses of aliquots of the same purified Ru solutions as "a", "b".

2.2. Ru chemical separation and purification

Iron meteorites, pallasites, and chondrites were dissolved in concentrated aqua regia, in a sealed Teflon vessel. Allende CAI were dissolved in Carius tubes with reverse aqua regia. Based on prior experience with Re–Os work, and on the absence of a residue, the samples were completely dissolved, although we can not guarantee that all SiC was dissolved. Ru was separated from sample solutions by ion-exchange and further purified by distillation techniques in order to remove Re, Mo, and Platinum Group Elements (PGE: Pd, Rh), which would potentially result in mass interferences on Ru isotopes. The ion-exchange techniques followed those described in a report by Rehkämper and Halliday (1997). Separation of Ru from the bulk matrix and quantitative recovery of other elements such as Zn, Cd, Ag, Pd, Re, Ir, and Pt were accomplished using

anion-exchange resin (AG 1 × 8, 100–200 mesh) in HCl and HNO_3. The analytical techniques for Ru distillation were similar to those for Re–Os (Chen et al., 1998).

2.3. Ru mass spectrometry

To establish the normal isotopic composition of Ru, we analyzed three Ru normals: (a) a specpure $RuCl_3$ standard solution; (b) a K_2RuCl_5 salt, reagent grade; and (c) a Ru-ammonium salt, $(NH_3)_5RuORu(NH_3)_4ORu(NH_3)_5Cl_6$, of 99.99% purity. In this study, we determined the Ru isotopic composition in terrestrial and meteorite samples using a new mass spectrometry laboratory at JPL, equipped with a Thermo-Finnigan Triton thermal ionization mass spectrometer, with 9 Faraday cups. We measured the negative oxides RuO_3^- within the mass range of 144–152 amu. It is beneficial, for ionization, to introduce oxygen (ultra-high purity) to the ion source region. We observe that for negative ions the emission is a very sharply defined function of the filament temperature, but not precisely defined, because it depends on the specifics of each sample filament load. For example, beam intensity grows relatively fast, once the optimum temperature for ion emission is reached, while we do not change the current through the filament. However, the optimum emission temperature is not precisely reproducible; hence, it is also not easy to specify the amount of oxygen introduced into the source through a micro-leak valve. It is also well known, that, if the optimum emission temperature is exceeded, ionization efficiency drops precipitously. For each experiment, about 100 ng, only, of pure Ru were loaded onto an outgassed Pt filament. This relatively low amount of Ru was enabled by the high ionization efficiency and transmission of Ru as a negative oxide ion. A mixture of $Ba(NO_3)_2$ and $Ba(OH)_2$ was used (in the approximate ratio of 1:10) as the negative ion emitter. The ion beam intensities for both terrestrial standards and meteorite samples ranged from 5×10^{-12} to 2×10^{-11} A, for $^{101}Ru^{16}O_3^-$, for more than 10 h. The typical ionization efficiency (ions collected divided by the atoms loaded on the filament and taking into account the ~50% transmission for the Triton) is estimated to be 4%. The oxygen isotopic composition was determined directly using $^{104}Ru^{i}O^{16}O_2^-$ ($i = 16, 17, 18$) and was constant during the runs. The oxygen isotope composition from RuO_3^- agrees within errors with that determined previously using $^{187}ReO_4^-$ (Shen et al., 1996). The following oxygen isotopic composition was used in reducing the Ru oxide data to the element data: $^{17}O/^{16}O = 0.00038$, $^{18}O/^{16}O = 0.002063$. We used a static mode to collect data by assigning $^{96-104}Ru^{16}O_3^-$ masses as follows: 144, 146, 147 to cups L3, L2, and L1; 148 to the Center cup; and 149, 150, and 152 to cups H1, H2, and H3. The amplifier gain calibration and amplifier noise and time response were performed prior to Ru isotopic measurements. Each sample analysis consisted of 5–6 mass spectrometer runs, using the same sample filament load, with each of these runs consisting of 270 ratios (ion beam integration of 16 s) obtained in sets of 10 ratios. The cup electrometers (9 in use) were "rotated" one position, every set of 10 ratios, following the practice recommended by the manufacturer. This allows bias from the electrometer gains to be averaged, but not eliminated.

The two p-process-only nuclides, ^{96}Ru and ^{98}Ru are difficult to measure precisely, because of their lower abundance (5.52% and 1.88%). The existence of abundant ^{96}Mo (16.7%) and ^{98}Mo (24.1%) isobars, which form MoO_3^- ions, required clean chemical separation of Ru from Mo, to eliminate mass interferences. In the absence of a clear choice for a pair of Ru isotopes for normalization for isotope fractionation (e.g., if Ru had two s-process only isotopes), we considered the magnitudes of the potential mass interferences for the $Ru^{16}O_3^-$ species. Interference from ^{100}Mo (9.63%) to the slightly more abundant ^{100}Ru (12.6%) is limited. In contrast, ^{99}Ru (12.7%) and ^{101}Ru (17%) are reasonably abundant and there are no Mo isobars or other known interfering elements or molecular species. Interferences from Ba (used as an emitter) at masses 150 and 152 ($^{134}Ba^{16}O$ and $^{136}Ba^{16}O$) to the two abundant Ru isotopes, $^{102}Ru^{16}O_3$ (31.6%) and $^{104}Ru^{16}O_3$ (18.7%) are negligible. We chose ^{101}Ru as the reference isotope and normalized our data to $^{99}Ru/^{101}Ru$ (instead of, for example, to $^{96}Ru/^{101}Ru$, as done by others), because: (1) ^{99}Ru is a factor of 2.3 more abundant than ^{96}Ru; (2) the choice of ^{99}Ru avoids the potential interference on ^{96}Ru from ^{96}Mo; and (3) there is no interference from Mo at mass 99 ($^{99}Ru^{16}O_3$ oxide mass 147). Based on these reasons, we consider the choice of $^{99}Ru/^{101}Ru$ for normalization as our preferred but clearly not unique choice. Other pairs of isotopes may be chosen. For example, for our normalization, potential effects in ^{99}Ru from ^{99}Tc decay would have propagated in easily calculable ways to the normalized Ru isotope ratios. Conversion from one normalization to another is simple, although it results in the propagation of the uncertainties of individual isotope ratios (cf. simple formulas in McCulloch and Wasserburg, 1978). A value of $^{99}Ru^{16}O_3/^{101}Ru^{16}O_3 = 0.741160$, derived from the mean ratios of Ru normals, was used to normalize the data, using the exponential law. For the application of the exponential law we found that use of the Ru oxide masses is most appropriate. After oxygen correction, the corresponding value for $^{99}Ru/^{101}Ru$ is 0.745075. We monitored MoO_3^- interferences (potentially at 140, 142, 143, 145) at the beginning and at the end of each run, using an electron multiplier, in the ion counting mode, with better than 85% efficiency. We have reduced and ultimately eliminated Mo isobaric interferences by using zone-refined, outgassed Pt filaments, and through careful clean-up chemistry for Ru. Any Ru data collected with $^{98}Mo^{16}O_3/^{98}RuO_3 > 5x10^{-5}$ were rejected. Mo interference at this level would yield, at most, an isobaric correction of 0.5 ε unit for ^{98}Ru. Possible interference from BaO was monitored at mass 153 ($^{137}Ba^{16}O$) and no corrections were needed nor applied.

3. ANALYTICAL RESULTS

In this study we report new high precision Ru isotopic compositions in chondrites, pallasites and iron meteorites using NTIMS techniques and an improved chemistry to minimize Mo isobaric interferences. Preliminary reports were presented at the Meteoritical Society Meeting (Chen and Papanastassiou, 2002) and Lunar and Planetary Science Conferences (Chen et al., 2003; Papanastassiou

et al., 2004). For this work, no mass interference corrections were needed and none was applied. For Ru, interferences from Mo would yield correlated positive shifts in ε_{96}, ε_{98}, and ε_{100} and from Ba, positive shifts in ε_{102} and ε_{104}.

3.1. Ru isotopic results

3.1.1. Precision and reproducibility

Three terrestrial standards were measured to establish the mass spectrometric techniques and the Ru normal composition. Once the techniques were established, mass spectrometer analyses of standards and samples were interleaved. At least one of the standards was measured before and after each meteorite sample measurement. A total of 1350–1620 ratios (ion beam integration 16 s per measurement) constitute a single analysis of about 100 ng Ru (sample or standard) loaded on a single filament. The mean and uncertainties (2σ) of each analysis are calculated after elimination of outliers (fewer than 5% of the measured cycles). The uncertainties reported for each analysis (Table 1) represent $2\sigma_{\text{mean}} = 2\sigma_N/\sqrt{n}$, where n is the number of ratios. This quoted uncertainty is the *internal precision* of an analysis, with the data obtained under similar conditions (e.g., ion signal intensity, range of mass-dependent isotope fractionation, absence of mass interferences, etc.). This uncertainty is used to confirm that an analysis is of high quality. However, it is also well established that for simultaneous ion collection, in state-of-the-art instruments, the reproducibility of isotope ratios between repeat analyses may be worse than the uncertainty obtained from the estimate of the internal precision of a single analysis. We consider that the true estimate of analytical precision is based on the "external" precision obtained for repeat analyses of the same Ru solution, which is our Ru terrestrial standard. The reproducibility/precision for the Ru isotope ratios is obtained as 2σ (and not $2\sigma_{\text{mean}}$) of the distribution of the analyses of the terrestrial Ru standards. The external uncertainties for terrestrial standards, measured for a period of about 11 months (April, 2002–February, 2003) are listed at the bottom of Table 1 and shown as uncertainty envelopes in Figs. 1 and 2 (dashed vertical lines). For comparison, the internal precision ($2\sigma_{\text{mean}}$) is listed for each sample analysis in Table 1, and is the same or slightly better than the external precision obtained for the standards. We consider the *external precision* for the standards (quoted at the 2σ level) as the correct estimate of uncertainty for all runs, which show good *internal precision*. The Ru isotopic compositions, after normalization to $^{99}Ru/^{101}Ru$, are expressed in ε-units, which are defined as the relative deviations of the measured (M) sample relative to the mean of the terrestrial Ru standards in parts in 10^4,

$$\varepsilon_i = \{[{}^{i}\text{Ru}/{}^{101}\text{Ru}]_{\text{M}}/[{}^{i}\text{Ru}/{}^{101}\text{Ru}]_{\text{std}} - 1\} \times 10^4,$$

where $i = 96$, 98, 100, 102, and 104. In considering possible, resolved isotope anomalies for Ru isotopes, for meteorite samples, we will compare deviations from the normal compositions with the external precision for terrestrial normals (2σ, not $2\sigma_{\text{mean}}$): ±1.19 εu for ^{96}Ru, ±1.98 εu for ^{98}Ru, ±0.31 εu for ^{100}Ru, ±0.64 εu for ^{102}Ru, and ±0.58 εu for ^{104}Ru. Since ^{100}Ru has a high abundance and is bounded by the two normalizing isotopes, ^{99}Ru and ^{101}Ru, the $^{100}Ru/^{101}Ru$ ratios are the most precise ($2\sigma = \pm 0.31$ εu). The uncertainties for $^{102}Ru/^{101}Ru$ and $^{104}Ru/^{101}Ru$ are two times larger, even though they are 2.5 and 1.5 times more abundant than ^{100}Ru. Some of the possible reasons are: (1) larger uncertainty for $^{104}Ru/^{101}Ru$ due to application of the fractionation correction over a larger mass range; (2) slight variations in cup factors (ion collection efficiency of the cup used) associated with Z-focusing effects because the distances of the cups used for these two isotopes are farther from the center cup; and (3) but least likely, interferences from $^{134}Ba^{16}O$ and $^{136}Ba^{16}O$. The data for the minor isotopes ^{98}Ru (1.86% relative abundance) and ^{96}Ru (5.54%) have larger uncertainties, which reflect the lower abundances and larger fractionation corrections (for a given fractionation factor per mass unit difference). The typical uncertainties (2σ) for $^{96}Ru/^{101}Ru$ and $^{98}Ru/^{101}Ru$ are 1.2 and 2 εu, respectively.

For comparison, in Table 1, the internal precision ($2\sigma_{\text{mean}}$) is listed for each sample analysis and is the same or better than the external precision, obtained for the standard. The only exception is provided by the data for the Pink Angel, fine-grained CAI, due to a limited amount of Ru. We also note that the 2nd analysis of Murchison is less precise because the data were obtained at low intensity. In this study, meteorite Ru data, which plot within the error envelopes of the terrestrial standards, are considered as having normal values.

3.1.2. Ru from chondrites and Allende CAI

We analyzed Ru from several ordinary chondrites (Olivenza, Portales Valley, Ransom and Garnet, Fig. 1) and two carbonaceous chondrites (Murchison and Allende, Fig. 1). Because the Ru concentrations in chondrites are one to two orders of magnitude lower than those in iron meteorites, the chondrite Ru data show larger uncertainties. Two whole-rock samples and a metal-rich separate of Olivenza yield normal Ru isotopic compositions and plot within the error envelopes of terrestrial standards. Similarly, metal from the metal-rich chondrite Portales Valley, and whole-rock samples from Ransom and Garnet yield normal Ru isotopic values. In contrast, duplicate analyses of bulk Murchison, though with larger errors, due to low ion beam intensities, yield normal ε_{96} and ε_{98}, but slightly positive ε_{100} (0.60 ± 0.31 and 0.59 ± 0.31), ε_{102} (0.73 ± 0.64 and 0.81 ± 0.64), and ε_{104} (1.14 ± 0.58 and 1.65 ± 1.02). Here we quote the *external precision* (see discussion in Section 3.1.1. above) derived from the Ru standards. If the *internal precision* of each measurement is larger than the external precision we use the internal precision. A whole-rock powder from Allende, prepared more than 30 years ago, was analyzed. Duplicate mass spectrometric analyses of the purified Ru (Allende WR1a and WR1b) yield reproducible large deficits in ε_{100} (-1.56 ± 0.31 and -1.70 ± 0.31). To verify this result, we prepared a new whole-rock powder from a slab of Allende (Allende WR2). This new sample yields a similar result ($\varepsilon_{100} = -1.23 \pm 0.31$) as the first sample, and confirms the relatively large ε_{100} deficit in Allende. The Allende WR samples also show hints of effects in ^{96}Ru, ^{98}Ru, and ^{104}Ru. We analyzed three

Table 1
Ru isotopic composition in meteorites.

Samples[a]		$^{96}Ru/^{101}Ru$[b]	±	$^{98}Ru/^{101}Ru$	±	$^{100}Ru/^{101}Ru$	±	$^{102}Ru/^{101}Ru$	±	$^{104}Ru/^{101}Ru$	±	ε_{96}[c]	±	ε_{98}	±	ε_{100}	±	ε_{102}	±	ε_{104}	±
Chondrites																					
Olivenza-1	LL5	0.321839	17	0.108916	17	0.737108	27	1.853427	18	1.097574	29	0.55	0.52	−0.84	1.52	0.44	0.36	0.31	0.10	−0.07	0.26
Olivenza-2	LL5	0.321846	30	0.108951	11	0.737069	9	1.853401	73	1.097592	57	0.77	0.94	2.44	1.03	−0.09	0.12	0.17	0.40	0.09	0.52
Olivenza-metal	LL5	0.321821	6	0.108935	6	0.737076	2	1.853453	20	1.097641	28	−0.01	0.19	0.93	0.52	0.00	0.02	0.45	0.11	0.54	0.25
Portales Valley	H4	0.321841	9	0.108942	7	0.737056	9	1.853290	15	1.097532	26	0.62	0.27	1.57	0.68	−0.26	0.12	−0.43	0.08	−0.45	0.24
Ransom	H4	0.321857	11	0.108947	13	0.737062	10	1.853401	13	1.097622	26	1.10	0.35	2.00	1.21	−0.19	0.14	0.17	0.07	0.37	0.24
Garnet	H4	0.321866	22	0.108939	7	0.737067	14	1.853385	28	1.097642	13	1.38	0.67	1.32	0.67	−0.12	0.19	0.08	0.15	0.55	0.12
Murchison-1	CM2	0.321835	22	0.108936	11	0.737120	12	1.853505	82	1.097707	62	0.44	0.67	1.08	1.02	0.60	0.16	0.73	0.44	1.14	0.56
Murchison-2	CM2	0.321831	28	0.108928	16	0.737119	22	1.853520	114	1.097763	112	0.31	0.87	0.34	1.46	0.59	0.30	0.81	0.61	1.65	1.02
Allende-1a	CV3	0.321852	8	0.108936	8	0.736960	6	1.853316	21	1.097645	15	0.96	0.25	1.05	0.70	−1.56	0.08	−0.29	0.11	0.58	0.14
Allende-1b	CV3	0.321825	11	0.108957	11	0.736950	3	1.853340	30	1.097671	46	0.13	0.34	2.94	0.99	−1.70	0.05	−0.16	0.16	0.82	0.42
Allende-2	CV3	0.321866	5	0.108949	6	0.736985	6	1.853328	19	1.097693	27	1.41	0.14	2.24	0.55	−1.23	0.09	−0.23	0.10	1.01	0.24
Allende CAI																					
Egg 3		0.321820	12	0.108934	11	0.736959	6	1.853370	27	1.097608	21	−0.05	0.37	0.87	0.97	−1.58	0.09	0.00	0.15	0.24	0.19
Egg 6		0.321850	24	0.108951	21	0.736959	15	1.853263	74	1.097524	99	0.88	0.74	2.37	1.94	−1.58	0.21	−0.58	0.40	−0.52	0.91
BigAl		0.321856	19	0.108940	5	0.736956	10	1.853303	23	1.097631	39	1.07	0.59	1.36	0.48	−1.63	0.13	−0.36	0.13	0.45	0.35
Pink Angel		0.321865	70	0.108914	36	0.737061	56	1.853469	113	1.097722	180	1.37	2.18	−1.03	3.29	−0.20	0.76	0.53	0.61	1.28	1.64
Irons																					
Canyon Diablo	IA	0.321846	22	0.108942	9	0.737076	24	1.853316	61	1.097571	49	0.77	0.69	1.62	0.83	0.00	0.33	−0.29	0.33	−0.10	0.45
Pitts	IB	0.321825	8	0.108923	6	0.737061	6	1.853361	21	1.097557	23	0.13	0.24	−0.19	0.57	−0.20	0.08	−0.05	0.11	−0.23	0.21
Bennett County	IIA	0.321842	19	0.108944	6	0.737020	6	1.853272	35	1.097534	47	0.63	0.58	1.79	0.55	−0.75	0.09	−0.53	0.19	−0.44	0.42
Negrillos	IIA	0.321845	14	0.108942	9	0.737039	11	1.853272	30	1.097541	43	0.74	0.45	1.59	0.85	−0.50	0.14	−0.53	0.16	−0.37	0.39
Coahuila	IIA	0.321803	13	0.108927	8	0.737037	12	1.853361	24	1.097610	35	−0.58	0.40	0.19	0.77	−0.53	0.16	−0.05	0.13	0.25	0.31
Cape York	IIIA	0.321834	10	0.108936	2	0.737031	4	1.853305	31	1.097534	32	0.40	0.33	1.06	0.17	−0.61	0.06	−0.35	0.17	−0.43	0.29
Grant	IIIB	0.321811	5	0.108923	7	0.737024	4	1.853323	20	1.097553	10	−0.31	0.15	−0.19	0.62	−0.70	0.05	−0.25	0.11	−0.26	0.09
Acuna	IIIB	0.321848	11	0.108944	8	0.737020	15	1.853290	33	1.097560	19	0.82	0.33	1.77	0.72	−0.76	0.21	−0.43	0.18	−0.19	0.18
Bella Roca	IIIB	0.321848	13	0.108937	2	0.737030	12	1.853271	35	1.097549	53	0.82	0.40	1.15	0.23	−0.62	0.16	−0.53	0.19	−0.30	0.49
Tres Castillos	IIIB	0.321834	11	0.108935	7	0.737039	6	1.853344	21	1.097576	19	0.39	0.35	0.95	0.66	−0.50	0.08	−0.14	0.11	−0.05	0.17
Gibeon	IVA	0.321837	17	0.108941	10	0.737046	4	1.853308	32	1.097555	26	0.51	0.53	1.46	0.91	−0.40	0.06	−0.34	0.18	−0.24	0.24
Hoba-1	IVB	0.321839	22	0.108924	6	0.736996	8	1.853314	34	1.097639	56	0.56	0.68	−0.11	0.59	−1.08	0.11	−0.30	0.18	0.52	0.51
Hoba-2a	IVB	0.321840	8	0.108935	7	0.737006	6	1.853323	17	1.097581	19	0.58	0.26	0.98	0.62	−0.95	0.09	−0.25	0.09	−0.01	0.17
Hoba-2b	IVB	0.321836	7	0.108939	3	0.737008	5	1.853318	20	1.097581	20	0.47	0.23	1.34	0.24	−0.91	0.06	−0.28	0.11	−0.01	0.18
Tlacotepec	IVB	0.321834	9	0.108932	7	0.737008	8	1.853349	18	1.097587	14	0.39	0.26	0.69	0.62	−0.92	0.10	−0.11	0.10	0.05	0.13
Pinon	UN	0.321827	11	0.108920	3	0.737014	8	1.853353	5	1.097591	26	0.17	0.35	−0.42	0.32	−0.83	0.11	−0.09	0.03	0.08	0.23
Pallasites																					
Salta	Pal	0.321835	5	0.108938	4	0.737046	6	1.853365	19	1.097579	15	0.43	0.17	1.20	0.35	−0.40	0.08	−0.03	0.10	−0.02	0.14
Springwater	Pal	0.321836	9	0.108942	11	0.737049	16	1.853399	24	1.097623	27	0.45	0.29	1.56	1.05	−0.36	0.22	0.15	0.13	0.37	0.25
Thiel Mountain	Pal	0.321828	6	0.108927	7	0.737033	4	1.853375	7	1.097561	15	0.20	0.19	0.25	0.61	−0.58	0.05	0.02	0.04	−0.19	0.14
Terrestrial standards																					
Mean		0.321821	38	0.108925	22	0.737076	23	1.853370	118	1.097582	63	0.00	1.19	0.00	1.98	0.00	0.31	0.00	0.64	0.00	0.58

[a] Number after meteorite names represents replicate analyses; letters after number represent multiple analyses of the same sample solution.
[b] Normalized to $^{99}Ru/^{101}Ru = 0.7450754$, using the exponential law; errors $= 2\sigma_{mean}$.
[c] $\varepsilon = (R_M/R_N - 1) \times 10^4$, R_M = measured ratios and R_N = mean of terrestrial normal. The typical ion intensity for $^{101}Ru^{16}O_3^-$ ranged from (0.5 to 2) $\times 10^{-11}$ A; the mass-dependent isotope fractionation ranged over 1‰ per amu. We observed no correlation of anomalies with the size of isotope fractionation and no deviations from the exponential law.

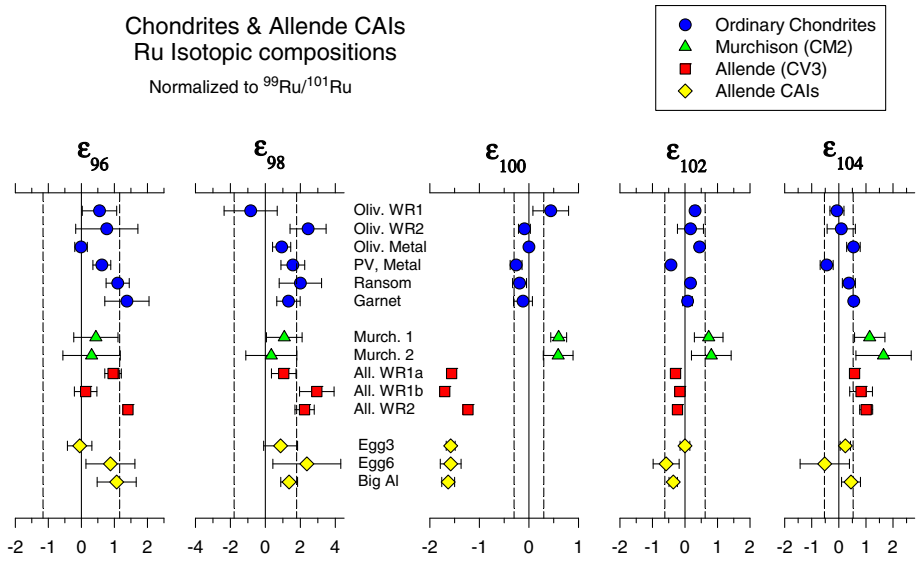

Fig. 1. Deviations of the Ru isotope compositions in chondrites and Allende CAI (in parts in 10^4). The uncertainties for normal Ru are given by the dashed vertical lines.

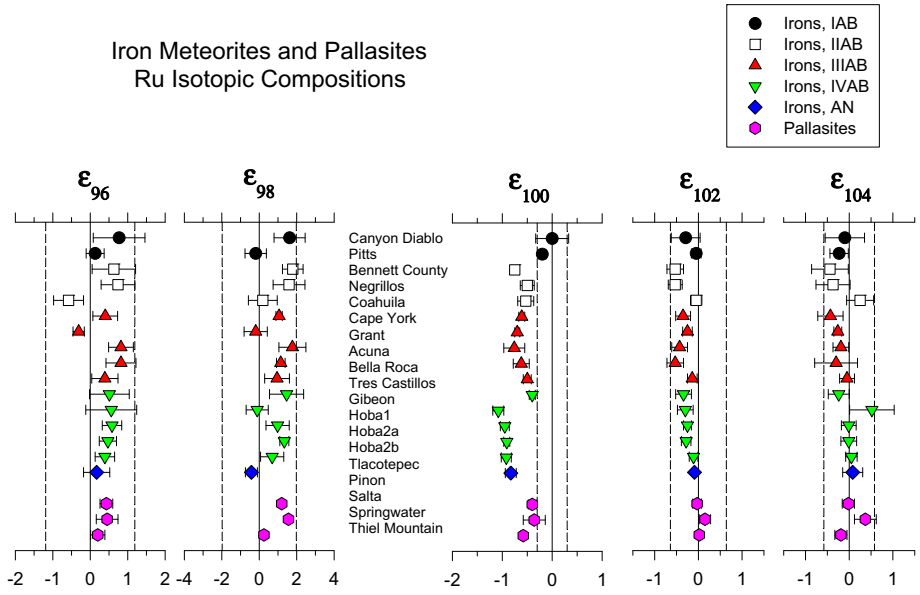

Fig. 2. Deviations of the Ru isotope compositions in iron meteorite and pallasite metals (in parts in 10^4). The uncertainties for normal Ru are given by the dashed vertical lines.

coarse-grained CAI from Allende (Egg 3, Egg 6, and Big Al, Fig. 1). The results indicate that all three CAI, have large, resolved deficits in ε_{100} (-1.58 ± 0.31 to -1.63 ± 0.31) and no other resolved effects. We also analyzed a fine-grained CAI from Allende (Pink Angel, Armstrong et al., 1981). The Ru concentration in the Pink Angel was much lower than in the coarse-grained CAI. The Ru isotopic composition was normal with larger uncertainties (Table 1).

3.1.3. Ru from FeNi metal in irons and pallasites

We analyzed two group IAB irons (Canyon Diablo and Pitts). They show no detectable deviations from normal Ru (Fig. 2). Three group IIAB irons (Bennett Co., Negrillos, and Coahuila, Fig. 2) show normal Ru isotopic ratios, except for clear deficits in $^{100}Ru/^{101}Ru$, from -0.50 ± 0.31 to -0.75 ± 0.31 εu. Five IIIAB irons (Cape York, Grant, Acuna, Bella Roca and Tres Castillos, Fig. 2) also show from -0.50 ± 0.31 to -0.76 ± 0.31 εu resolved deficits in the $^{100}Ru/^{101}Ru$ ratio, and normal values in all other Ru isotopic ratios. Similarly, iron meteorite data of groups IVA (Gibeon), IVB (Hoba and Tlacotepec) and an AN (ungrouped) iron (Piñon) are shown in Fig. 2. From the IVA and IVB irons, Gibeon shows a small shift in $^{100}Ru/^{101}Ru$ ratio ($\varepsilon_{100} = -0.40 \pm 0.31$), while Hoba-1 (Table 1) yields one of the larger deficits for the $^{100}Ru/^{101}Ru$ ratio ($\varepsilon_{100} = -1.08 \pm$

0.31). To verify this result, we dissolved another piece of this meteorite (Hoba-2) and determined the Ru isotopic composition. The results on Hoba-2 (Hoba-2a, Table 1), show $\varepsilon_{100} = -0.95 \pm 0.31$, which is in excellent agreement with the first determination. An aliquot (Hoba-2b) of the Hoba-2 solution was processed twice through the ion-exchange and distillation steps to improve potentially the purity on Ru. Hoba-2b yields exactly the same Ru isotopic value within uncertainties ($\varepsilon_{100} = -0.91 \pm 0.31$) as Hoba-2a and confirms reproducible, well-resolved deficits in $^{100}Ru/^{101}Ru$, observed in triplicate for Hoba. Another IVB iron, Tlacotepec, also yields negative $\varepsilon_{100} = -0.92 \pm 0.31$. Piñon (AN group) yields negative $\varepsilon_{100} = -0.83 \pm 0.31$. Analyses of three pallasites (Salta, Springwater, and Thiel Mountain, Fig. 2) yield slightly negative ε_{100}, which range from -0.36 ± 0.31 to -0.58 ± 0.31. For all meteorites discussed up to now (Figs. 1 and 2), we also note that ε_{96} and ε_{98} typically show small, positive values, although they are not resolved from normal, within the larger, observed uncertainties for these isotopes.

In summary, we find no Ru isotopic effects in the ordinary chondrites and group IAB iron meteorites, which we measured. With these exceptions, there are endemic deficits in ^{100}Ru in iron meteorites (Groups IIAB, IIIAB, IVA, IVB, and AN) and possibly in pallasites. There are significant effects in ^{100}Ru in whole-rock samples of carbonaceous chondrites and in Allende coarse-grained refractory inclusions. The Murchison whole-rock samples show small hints of excesses in $^{100,102,104}Ru$, which are not clearly resolved, but which appear distinct from the endemic deficits in ^{100}Ru, for irons and the Allende WR and CAI.

4. DISCUSSION

4.1. Reported Ru isotopic data in the literature

Poths et al. (1987), using a positive ion TIMS (PTIMS) technique, obtained Ru isotope data on CAI from the Allende and Leoville carbonaceous chondrites. For their normalization to $^{96}Ru/^{101}Ru$, they obtained normal abundances for ^{98}Ru and ^{99}Ru in CAI with large uncertainties (2σ) of ± 10 and ± 2.6 εu, respectively. Resolved excesses for ^{104}Ru were attributed by these authors to potential contamination from a ^{104}Ru tracer, used in their work. Ion microprobe studies on refractory metal nuggets from Allende refractory CAI (at percent level precision) showed normal Mo and Ru isotopic compositions (Hutcheon et al., 1987). Yin et al. (1992) employed NTIMS, to determine the Ru isotopic composition in terrestrial and meteoritic samples. Normalizing data to $^{96}Ru/^{101}Ru$, they found a small positive deviation of 0.89 ± 0.24 εu, for $^{99}Ru/^{101}Ru$ in the magnetic fraction of the carbonaceous chondrite Maralinga, but no deviation in the whole-rock. Using NTIMS, Smoliar (1998) reported, in an abstract, variable excesses only for ^{98}Ru of up to 40 εu (normalized to $^{100}Ru/^{101}Ru$) in Group IIA, IIIA, and IVB iron meteorites, but provided no analytical details on isobaric interference corrections. In the absence of supporting information or follow up work, and given the disagreement between data reported by Becker and Walker (2003a, see below) and in this work, the report by Smoliar (1998) will not be considered further. Using NTIMS and normalized to $^{100}Ru/^{101}Ru$, Becker and Walker (2000) indicated that there were *barely* resolvable but reproducible positive ^{98}Ru anomalies in IIAB and IIIA iron meteorites, after correction for small interferences from ^{98}Mo, and possibly small positive anomalies in ^{99}Ru. However, in subsequent reports, Becker and Walker (2001, 2002, 2003a) and Becker et al. (2002) indicated that in iron meteorites and chondrites, no resolvable isotopic effects were found with a precision of ± 0.8 εu for $^{98}Ru/^{101}Ru$ and ± 0.3 εu for $^{99}Ru/^{101}Ru$, and suggested that the effects reported in their previous study (Becker and Walker, 2000) were most likely analytical artifacts. Although these Ru analyses, using NTIMS, yielded more precise Ru data, they required substantial corrections for mass interferences. We note that the study of Becker and Walker (2003a) was a focused search for possible radiogenic effects in Ru from the decay of ^{98}Tc and ^{99}Tc. For this study, they normalized their data to $^{96}Ru/^{101}Ru$ and they did not report data on ^{100}Ru, ^{102}Ru, or ^{104}Ru. Hence, a comparison with our data is possible only for $^{98}Ru/^{101}Ru$ and $^{99}Ru/^{101}Ru$. For this comparison, we recalculated our data to a $^{96}Ru/^{101}Ru$ normalization. For this normalization we also obtain normal values for $^{98}Ru/^{101}Ru$ and $^{99}Ru/^{101}Ru$. In order to avoid propagation of uncertainties through the renormalization, we estimate our uncertainty for $^{98}Ru/^{101}Ru$ to be the same (i.e., 2 εu) as for our standard normalization. For $^{99}Ru/^{101}Ru$, we assume that the uncertainty is the same as for $^{100}Ru/^{101}Ru$ (i.e., 0.3 εu). With these uncertainty estimates, our renormalized values for ^{98}Ru and ^{99}Ru are normal and, hence, there is no significant disagreement between our data and the data of Becker and Walker (2003a), based on the same normalization, and for this restricted set of Ru isotopes, based on the data they reported. While both sets of data indicate normal $^{98,99}Ru$, our values for terrestrial Ru indicate that $^{98}Ru/^{101}Ru$ and $^{99}Ru/^{101}Ru$ are 1.35 εu lower and 0.72 εu higher, respectively, than Becker and Walker (2003a). We also emphasize that it is not possible to compare data for ^{100}Ru, ^{102}Ru, and ^{104}Ru.

The data we have presented are free from interfering species and not subject to added uncertainties for corrections for mass interferences.

4.2. Ru isotopic anomalies in meteorites and s-process nucleosynthesis

We now consider the endemic anomalies in ^{100}Ru. For the normalization used, we observe up to 1.7 εu depletion in the pure s-process isotope, ^{100}Ru. More specifically, samples of the Allende whole-rock and of three coarse-grained inclusions show relatively large and similar deficits for ^{100}Ru from -1.23 to -1.7 εu. FeNi metal from iron meteorites in groups IIAB, IIIAB, IVA, IVB, and AN show deficits from -0.4 to -1.08 εu, with the IVB irons (Hoba and Tlacotepec) having the largest effects of -0.91 to -1.08 εu. Three pallasites show hints of small effects, while ordinary chondrites and group IAB irons show normal Ru isotope composition, for the samples analyzed. The presence of Ru isotopic effects is clearly resolved, but the attribution of the isotope anomalies to specific isotopes depends on the choice of normalization for isotope fractionation. For the normalization we have chosen, we consider first the Ru isotope patterns that would result from an exotic s-pro-

cess component (excess or deficit). For this, we calculate the Ru isotopic pattern for the terrestrial Ru depleted in the s-process Ru isotopes with a composition for the s-process isotopes as calculated by Arlandini et al. (1999).

For illustration we consider the Hoba and the Allende WR data, in detail. Similar calculations apply to the other samples, which show clear ^{100}Ru deficits. In Fig. 3a, we show the isotopic pattern for terrestrial Ru depleted by 0.14‰ in s-process Ru isotopes and normalized to ^{99}Ru/^{101}Ru. This calculation produces a deficit of $\varepsilon_{100} = -1.08$ εu, reproducing the deficit observed in Hoba-1. The calculated pattern for all Ru isotopes shows good agreement with that of Hoba-1. We also show the experimental uncertainties for normal Ru (grey lines, Fig. 3). No apparent effects are resolved for Ru isotopes, except for ^{100}Ru, at the limit of resolution, based on the range of uncertainty for normal Ru. Similarly, we show in Fig. 3b the Ru isotope patterns for a depletion of 0.22‰ in s-process Ru isotopes to generate a deficit of −1.7 εu at ^{100}Ru, for the normalized composition, as observed for Allende-1b. The patterns for the calculated data and Allende-1b also show a good agreement. These considerations demonstrate that an observable and well-resolved but small effect at ^{100}Ru can be due to an s-process deficit, without the rest of the Ru isotopes showing resolvable anomalies, based on the current level of precision. However, based on the size of the ^{100}Ru effects, the s-process mixing calculations

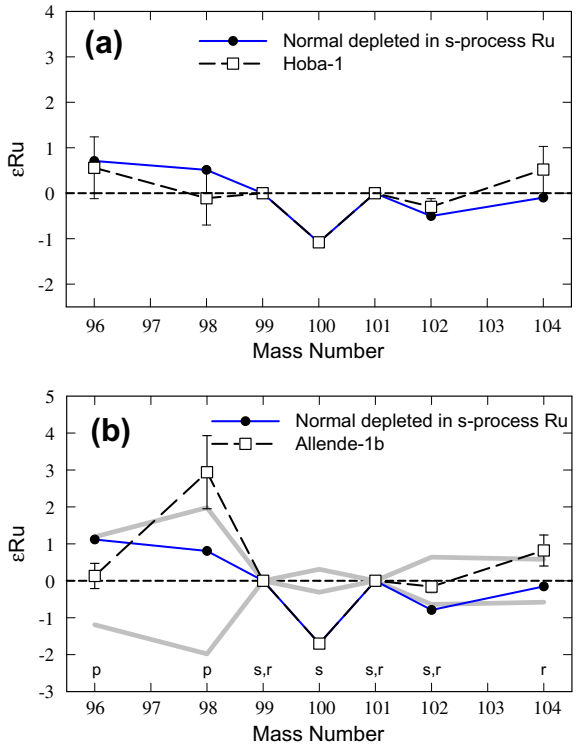

Fig. 3. A comparison of the isotopic patterns for meteorites (squares) and terrestrial Ru depleted in s-process Ru isotopes (circles) to produce the observed deficits in ^{100}Ru in two meteorites: (a) Hoba-1 and the calculated pattern for 0.14‰ depletion in s-process Ru isotopes: the effects are matched at $\varepsilon_{100} = -1.08$ εu; and (b) Allende WR1b and 0.22‰ depletion in s-process Ru isotopes: the effects are matched at $\varepsilon_{100} = -1.7$ εu. All patterns are normalized to ^{99}Ru/^{101}Ru.

predict also a small, resolvable deficit in ^{102}Ru which was not observed in all of our samples. The absence of endemic small effects in ^{102}Ru in our data, in opposition to the s-process calculations, in this mass region, point to a need for re-examination of the detailed s-process neutron capture cross sections and calculations. The observed Ru isotope patterns are, to first order, consistent with an observed (for the isotope pattern normalized for mass fractionation) s-process deficit for ^{100}Ru of up to 1.7 εu, which implies an overall deficit in the s-process component of up to 0.22‰. In addition, apparent excesses in ^{98}Ru are observed also in other measurements of the same samples (Allende-1a and -2). Even though effects at ^{96,98}Ru are not well-resolved, the Allende data suggest that excesses in ^{98}Ru are larger than excesses in ^{96}Ru. The s-process mixing calculations show small excesses in both ^{96}Ru and ^{98}Ru with a slightly higher excess for ^{96}Ru, relative to ^{98}Ru. This would imply that the observed patterns for ^{96,98}Ru in Allende are not simply a reflection of the s-process deficit, but result also from addition of a p-process component depleted in ^{96}Ru and enhanced in ^{98}Ru or reflect possible effects from ^{98}Tc (see below). Similarly, the effects in ^{104}Ru, especially for Murchison and Allende whole-rock samples, while not clearly resolved, suggest the presence of an excess in r-process, above the level in solar system materials. We note that the data on bulk Murchison suggest excesses in ^{100}Ru and in ^{104}Ru, which are distinct from the rest of the measured patterns. We also note that the Pink Angel shows no resolved effects in Ru, even though it has well-resolved Mo isotope anomalies, corresponding to an s-process excess (Chen et al., 2004). However, the Ru isotopic composition in this sample is less precisely determined due to the lower Ru abundance in the Pink Angel.

Savina et al. (2004) have presented Ru on many SiC pre-solar grains and have also provided nucleosynthetic calculations of the s-process in 1.5 and 3 solar mass stars. The data on pre-solar grains are fully consistent with a dominant s-process component. The effects measured on these grains are large and unambiguous. The data on SiC also showed an excess in ^{99}Ru, above the s-process calculated component. This was interpreted by Savina et al. (2004) to be consistent with the presence of effects from the in situ decay of ^{99}Tc. In contrast to the large and clear s-process component in pre-solar grains, the small endemic effects observed in bulk samples of carbonaceous meteorites, refractory inclusions, and planetary differentiates, such as the magmatic group iron meteorites correspond to deficits in s-process components. If the pre-solar grains constitute a significant, identifiable contribution to the solar system, then the materials we have analyzed did not receive their full complement of s-process Ru, as measured in the pre-solar SiC grains. It is highly unlikely that our sample dissolution techniques did not dissolve SiC particles in the carbonaceous meteorites or that SiC were preserved in magmatic irons and not dissolved by our procedures.

4.3. Effects of different normalization methods on Ru isotopic patterns

Based on the endemic ^{100}Ru isotope effects, it is reasonable to interpret the observed patterns for Ru as due to an s-process deficit, with potentially also a non-solar p-process

component. We consider below also different possible exotic components based on different normalization conventions for the data. Different normalization conventions effectively rotate the isotope patterns to yield correlated effects in different Ru isotopes. In Fig. 4, we used the Hoba-1 data to demonstrate the effect of different mass fractionation normalizations:

4.3.1. Case 1 scenario: normalization to $^{99}Ru/^{101}Ru$

For Hoba-1, for the ^{99}Ru-^{101}Ru normalization, we have used, we obtain normal Ru isotope ratios except for the well-resolved deficit in ^{100}Ru/^{101}Ru ($\varepsilon_{100} = -1.08 \pm 0.31$, Fig. 4a and b, circles). Subtracting from normal Ru 0.14‰ of ^{100}Ru with an s-process isotopic abundance pattern and after renormalization using ^{99}Ru/^{101}Ru, we obtain a similar pattern as Hoba-1 (Fig. 3a). Therefore, the negative shift in ^{100}Ru in Hoba and other meteorites seems to be best explained by having a deficit in the s-process component.

4.3.2. Case 2 scenario: Normalization to $^{100}Ru/^{101}Ru$

Normalization to ^{100}Ru/^{101}Ru (Fig. 4a, squares) results in rotating (clockwise) the isotope pattern, and yields large enrichments (5.9 and 3.2 εu) in the two p-process isotopes (^{96}Ru and ^{98}Ru) and a +2.2 εu effect in r- and s-process ^{99}Ru. It also yields large depletions in the r- and s-process ^{102}Ru (−1.3 εu) and in the pure r-process ^{104}Ru (−2.7 εu). This normalization would require the presence of both p-process excesses and r-process deficits for Ru.

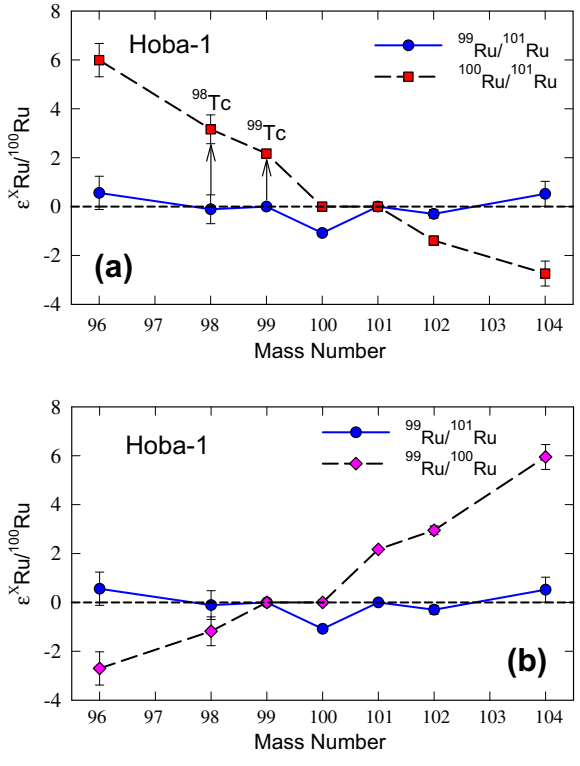

Fig. 4. Effects of different mass fractionation normalizations to the Hoba data. The Ru data normalized to ^{99}Ru/^{101}Ru are shown as open circles. The isotopic patterns using other isotopic ratios to normalize the Ru data are shown in (a) ^{100}Ru/^{101}Ru (squares) and (b) ^{99}Ru/^{1001}Ru (diamonds).

Case 2 suggests that short-lived nuclei ^{98}Tc and ^{99}Tc could have been alive when Hoba (and other meteorites) was formed. The requirements for the positive shift in ^{98}Ru and ^{99}Ru from ^{98}Tc and ^{99}Tc decays are: (1) production and preservation of live ^{98}Tc and ^{99}Tc in the early solar system; (2) significantly large relative production yield ratio or large fractionation of Tc/Ru in parent bodies while ^{98}Tc and ^{99}Tc are still alive; and (3) efficient separation and preservation of these highly fractionated Tc/Ru reservoirs. An excess in ^{99}Ru of 2.2 εu, for this normalization to ^{100}Ru/^{101}Ru, corresponds to a very high ^{99}Tc/^{100}Ru of 2.2×10^{-4}, as compared to a solar system initial ratio of 3.4×10^{-5} calculated by Wasserburg et al. (1994). This would require a significant fractionation for Tc/Ru, for which there is little support (cf. Becker and Walker, 2003a). Given the very short half-life of ^{99}Tc, the radiogenic ^{99}Ru would have had to be preserved in refractory metal condensates and been incorporated in FeNi (see below). These arguments do not provide support for a normalization of the Ru data to ^{100}Ru/^{101}Ru.

4.3.3. Case 3 scenario: Normalization to $^{99}Ru/^{100}Ru$

For Case 3, we normalize the Hoba Ru data to ^{99}Ru/^{100}Ru (Fig. 4b, squares) which corresponds to a counter-clockwise rotation of the relative isotope ratios and obtain depletions in the two p-process nuclides, ^{96}Ru (−1.2 εu) and ^{98}Ru (−2.7 εu), large enrichments in two r- and s-process nuclides, ^{101}Ru (2.2 εu) and ^{102}Ru (3.0 εu) and a very large enrichment in the pure r-process nuclide ^{104}Ru (5.9 εu). This implies an inhomogeneous mixing process, which introduced an overabundance in the s- and r-process nuclides, but an under abundance in the p-process nuclides.

We still consider Case 1 the preferred normalization procedure leading to endemic effects (deficits) in ^{100}Ru and an endemic deficit is s-process Ru.

4.4. Comparison of Ru and Mo isotopes

Dauphas et al. (2002) reported molybdenum isotopic anomalies in differentiated and bulk primitive meteorites. Yin et al. (2002) also reported Mo isotopic anomalies in carbonaceous chondrites and Allende CAI. We have also reported Mo isotopic anomalies in carbonaceous chondrites and Allende CAI (Chen et al., 2004). In contrast, Becker and Walker (2003a,b) reported uniform solar system Mo and Ru isotopic compositions. Dauphas et al. (2004) showed that, when bulk measurements are grouped by meteorite class, there is a good correlation between their ε^{92}Mo data and our ε^{100}Ru data (Chen et al., 2003; Papanastassiou et al., 2004) as expected from nucleosynthesis theory. They also indicated that the remarkable agreement in the Ru–Mo correlation between the meteorite data and the one predicted by nucleosynthesis theory confirmed that the isotopic anomalies observed in meteorites resulted from variations in the s-process contributions. While most of the iron meteorites lie along the Ru–Mo correlation line, the main group pallasites and CV chondrites (e.g., Allende and Murchison) do not plot on this line. Fujii et al. (2006) indicated that the mass-independent anomalies of Mo and Ru observed in Murchison show a strong correla-

tion with the nuclear charge distribution. They argued that *some* of the isotopic anomalies observed in meteorites may be due to a nuclear field shift rather than nucleosynthetic processes. More work is needed to understand the meaning and the relationship between bulk meteorites Mo, Zr, and Ru isotopic data and pre-solar SiC grains.

4.5. Preservation of endemic Ru anomalies

We have determined endemic effects in Ru, which, with a normalization to $^{99}Ru/^{101}Ru$, correspond to deficits of up to 1.7 εu in Allende and up to 1.1 εu in Hoba, in the s-process-only ^{100}Ru. The work by Savina et al. (2004) on Ru in SiC interstellar grains yields the s-process pattern, with very large depletions of p- and r-process Ru isotopes and evidence for Tc. However, while the results on SiC grains are impressive, at this time it is unclear what the major carriers of refractory siderophiles are. The question is why Ru (and Mo) should show endemic effects in planetary differentiates. If endemic isotope anomalies for Ru were the norm in the early solar system, we would have expected effects also in chondrites and for many other elements which are mixtures of s- and r-process isotopes. A possible mechanism would be to have all the refractory siderophile elements condense out as micro-particles or nuggets very early in the solar nebula and at a sufficiently early time to still preserve initial isotope heterogeneities. Then these refractory siderophile condensates or nuggets could get trapped in the condensing FeNi, at relatively high temperatures (Kelly and Larimer, 1977). In any subsequent planetary differentiation, the refractory siderophiles would stay in the FeNi, throughout the process. Hence, an initial isotope heterogeneity in the earliest refractory siderophile condensates would be preserved through a FeNi planetary differentiation process. The question still remains for the mechanism to preserve isotope heterogeneity for very fine-grained, early refractory siderophile condensates. Such preservation has occurred for many refractory elements in Ca–Al-rich inclusions. If enough s-process Ru came into the solar system as SiC, from AGB stars, that would be a way to leave out some s-process Ru from the highly siderophile condensates as they became trapped or acted as condensation centers for FeNi. Then the SiC would be trapped by the silicate phases coming out (or at least SiC was not trapped equally well by FeNi). One way to investigate this issue is to apply these high sensitivity and precision techniques to Fremdlinge and metal nuggets found in CAI. An attempt was made by Hutcheon et al. (1987), but the present techniques need to be used. At this time it is not possible to predict whether refractory metal nuggets from CAI should show excesses or deficits in s-process Ru.

5. CONCLUSIONS

We find no Ru isotopic effects in ordinary chondrites and in non-magmatic, group IAB iron meteorites. There are significant effects, corresponding to deficits in the pure s-process nuclide ^{100}Ru, in the Allende whole-rock and refractory inclusions. There are also endemic deficits in ^{100}Ru in magmatic iron meteorites and possibly in pallasites. The current Ru data suggest a wide spread and large scale deficit in s-process nuclides or enhancements in both p- and r-process nuclides in the early solar nebula. In contrast, the data on bulk Murchison suggest an excess in ^{100}Ru and in ^{104}Ru, which are distinct from the rest of the measured patterns. Our current Ru results on iron meteorites do not show effects in ^{99}Ru, which could correlate with ^{107}Pd as inferred from excess in ^{107}Ag in iron meteorites and pallasites (Chen and Wasserburg, 1996). This is consistent with the short half-life of ^{99}Tc and the much smaller expected chemical fractionation for Tc/Ru, relative to the volatility-controlled Pd/Ag fractionation.

ACKNOWLEDGMENTS

We thank Rasmus Andreasen, Andrew Davis, and Laurence Nyquist for constructive reviews of the paper. J.H.C. and the laboratories at J.P.L. were supported by NASA Cosmochemistry; D.A.P. was supported by J.P.L. (RTD); and G.J. Wasserburg was supported by NASA Cosmochemistry through J. Nuth.

REFERENCES

Andreasen R. and Sharma M. (2006) Solar nebula heterogeneity in p-process Samarium and Neodymium isotopes. *Science* **314**, 806–809.

Andreasen R. and Sharma M. (2007) Mixing and homogenization in the early solar system: clues from Sr, Ba, Nd, and Sm isotopes in meteorites. *Ap. J.* **665**, 874–883.

Arlandini C., Wisshak F., Käppeler K., Gallino R., Lugaro M., Busso M. and Straniero O. (1999) Neutron capture in low-mass asymptotic giant branch stars: cross sections and abundance signatures. *Ap. J.* **525**, 886–900.

Armstrong J. T., Papanastassiou D. A. and Wasserburg G. J. (1981). The Allende Pink Angel: Its mineralogy, petrography and the constraints of its genesis. *Lunar Planet. Sci. Conf. XII*, pp. 25–28.

Barzyk J. G., Savina M. R., Davis A. M., Gallino R., Pellin M. J., Lewis R. S., Amari S. and Clayton R. N. (2006) Multi-element isotopic analysis of single presolar SiC grains. *New Astro. Rev.* **50**, 587–590.

Barzyk J. G., Savina M. R., Davis A. M., Gallino R., Gyngaard F., Amari S., Zinner E., Pellin M. J., Lewis R. S. and Clayton R. N. (2007) Constraining the ^{13}C neutron source in AGB stars through isotopic analysis of trace elements in presolar SiC. *Meteorit. Planet. Sci.* **42**, 1103–1119.

Becker H. and Walker R. J. (2000) Positive ^{98}Ru and ^{99}Ru anomalies in iron meteorites. *Lunar Planet. Sci. Conf. XXXI*. Lunar Planet. Inst., Houston. #1484.

Becker H. and Walker R. J. (2001) The ^{98}Tc–^{98}Ru and ^{99}Tc–^{99}Ru chronometers: new results on iron meteorites and terrestrial Ru. *Eleventh Annual V.M. Goldschmidt Conf*. Lunar Planet. Inst., Houston. # 3047.

Becker H. and Walker R.J. (2002) Ruthenium isotopic composition of terrestrial materials, iron meteorites and chondrites. *Lunar Planet. Sci. Conf. XXXIII*. Lunar Planet. Inst., Houston. #1018.

Becker H. and Walker R. J. (2003a) In search of extant Tc in the early solar system: Ru-98 and Ru-99 abundances in iron meteorites and chondrites. *Chem. Geol.* **196**, 43–56.

Becker H. and Walker R. J. (2003b) Efficient mixing of the solar nebula from uniform Mo isotopic composition of meteorites. *Nature* **425**, 152–155.

Becker H., Dalpe C. and Walker R. J. (2002) High-precision Ru isotopic measurements by multi-collector ICP-MS. *Analyst* **127**, 775–780.

Brandon A. D., Humayun M., Puchtel I. S., Leya I. and Zolensky M. (2005) Osmium isotope evidence for an s-process carrier in primitive chondrites. *Science* **309**, 1233–1236.

Carlson R. W., Boyet M. and Horan M. (2007) Chondrite barium, neodymium, and samarium isotopic heterogeneity and early earth differentiation. *Science* **316**, 1175–1178.

Chen J. H. and Papanastassiou D. A. (2002) NTIMS determination of ruthenium isotopes. 65th Annual Meteoritical Society Meeting. *Meteorit. Planet. Sci.* **37**, A31.

Chen J. H. and Wasserburg G. J. (1996) Live ^{107}Pd in the early solar system and implications for planetary evolution. In *Earth Processes: Reading the Isotopic Code*, vol. Geophysical Monograph 95 (eds. A. Basu and S. Hart). AGU, pp. 1–20.

Chen J. H., Papanastassiou D. A. and Wasserburg G. J. (1998) Re–Os systematics in chondrites and the fractionation of the platinum group elements in the early solar system. *Geochim. Cosmochim. Acta* **62**, 3379–3392.

Chen J. H., Papanastassiou D. A. and Wasserburg G. J. (2003) Endemic Ru Isotopic anomalies in meteorites. *Lunar Planet. Sci. Conf. XXXIV*. Lunar Planet. Inst., Houston. #1789.

Chen J. H., Papanastassiou D. A., Wasserburg G. J. and Ngo H. H. (2004) Endemic Mo isotopic anomalies in iron and carbonaceous meteorites. *Lunar Planet. Sci. Conf. XXXV*. Lunar Planet. Inst., Houston. #1431.

Dauphas N., Marty B. and Reisberg L. (2002) Molybdenum evidence for inherited planetary scale isotope heterogeneity of the protosolar nebula. *Ap. J.* **565**, 640–664.

Dauphas N., Davis A. M., Marty B. and Reisberg L. (2004) The cosmic molybdenum ruthenium isotope correlation. *Earth Planet. Sci. Lett.* **226**, 465–475.

Davis A. M., Lugaro M., Gallino R., Pellin M. J., Lewis R. S. and Clayton R. N. (2001) Isotopic compositions of heavy elements in presolar grains: new constraints on nucleosynthesis. *Mem. Soc. Astron. Ital.* **72**, 413–421.

Fehr M. A., Rehkämper M., Halliday A. N., Schönbächler M., Hattendorf B. and Gunther D. (2006) Search for nucleosynthetic and radiogenic tellurium isotope anomalies in carbonaceous chondrites. *Geochim. Cosmochim. Acta* **70**, 3436–3448.

Firestone R. B. and Shirley V. S. (1996) *Table of the Isotopes*. Wiley, New YorkGreenwood N. N. and Earnshaw A. () *Chemistry of the Elements*. Pergamon, Oxford, p. 1542.

Fujii T., Moynier F. and Albarède F. (2006) Nuclear field vs. nucleosynthetic effects as cause of isotopic anomalies in the early solar system. *Earth Planet. Sci. Lett.* **247**, 1–9.

Hutcheon I. D., Armstrong J. T. and Wasserburg G. J. (1987) Isotopic studies of Mg, Fe, Mo, Ru and W in Fremdlinge from Allende refractory inclusions. *Geochim. Cosmochim. Acta* **51**, 3175–3192.

Kelly W. R. and Larimer J. W. (1977) Chemical fractionations in meteorites-VIII. Iron meteorites and the cosmochemical history of the metal phase. *Geochim. Cosmochim. Acta* **41**, 93–111.

Kobayashi T., Sueki K., Ebihara M., Nakahara M., Imamura M. and Masuda A. (1993) Half-lives of technetium-97, technetium-98. *Radiochim. Acta* **63**, 29–31.

Lee D.-C. and Halliday A. N. (1995) Hf-W chronometry and the timing of terrestrial core formation. *Nature* **378**, 771–774.

Lee D.-C. and Halliday A. N. (2000) Accretion of primitive planetesimals: Hf-W isotopic evidence from enstatite chondrites. *Science* **288**, 1629–1631.

Lugaro M., Davis A. M., Gallino R., Pellin M. J., Straniero O. and Käppeler F. (2003) Isotopic compositions of Sr, Zr, Mo and Ba in single presolar SiC grains and Asymptotic Giant Branch stars. *Ap. J.* **593**, 486–508.

Lugmair G. W. and Galer S. J. G. (1992) Age and isotopic relationships among the angrites Lewis Cliff 86010 and Angra dos Reis. *Geochim. Cosmochim. Acta* **56**, 1673–1694.

Marhas K. K., Hoppe P. and Ott U. (2007) NanoSIMS studies of Ba isotopic compositions in single presolar silicon carbide grains from AGB stars and supernovae. *Meteorit. Planet. Sci.* **42**, 1077–1101.

McCulloch M. T. and Wasserburg G. J. (1978) Ba and Nd isotopic anomalies in the Allende meteorite. *Ap. J.* **220**, L15–L19.

Nicolussi G. K., Pellin M. J., Lewis R. S., Davis A. M., Amari S. and Clayton R. N. (1998a) Molybdenum isotopic composition of individual presolar silicon carbide grains from the Murchison meteorite. *Geochim. Cosmochim. Acta* **62**, 1093–1104.

Nicolussi G. K., Pellin M. J., Lewis R. S., Davis A. M., Clayton R. N. and Amari S. (1998b) Strontium isotopic composition in individual circumstellar silicon carbide grains: a record of s-process nucleosynthesis. *Phys. Rev. Lett.* **81**, 3583–3586.

Nicolussi G. K., Pellin M. J., Lewis R. S., Davis A. M., Clayton R. N. and Amari S. (1998c) Zirconium and molybdenum in individual circumstellar graphite grains: new isotopic data on the nucleosynthesis of heavy elements. *Ap. J.* **504**, 492–499.

Nyquist L. E., Bansal B., Wiesmann H. and Shih C. Y. (1994) Neodymium, strontium and chromium isotopic studies of the LEW86010 and Angra DOS Reis meteorites and the chronology of the angrite parent body. *Meteoritics* **29**, 872–885.

Papanastassiou D. A., Chen J. H. and Wasserburg G. J. (2004) More on Ru endemic isotope anomalies in meteorites. *Lunar Planet. Sci. Conf. XXXV*. Lunar Planet. Inst., Houston. #1828.

Poths H., Schmitt-Strecker S. and Begemann F. (1987) On the isotopic composition of ruthenium in the Allende and Leoville carbonaceous chondrites. *Geochim. Cosmochim. Acta* **51**, 1143–1149.

Ranen M. C. and Jacobsen S. B. (2006) Barium isotopes in chondritic meteorites: implications for planetary reservoir models. *Science* **314**, 809–812.

Rehkämper M. and Halliday A. N. (1997) Development and application of new ion-exchange techniques for the separation of the platinum group and other siderophile elements from geological samples. *Talanta* **44**, 663–672.

Reisberg L. C., Dauphas N., Luguet A., Pearson D. G. and Gallino R. (2007) Large s-process and mirror osmium isotopic anomalies within the Murchison meteorite. *Lunar Planet. Sci. Conf. XXXVIII*. Lunar Planet. Inst., Houston. #1177.

Reisberg L. C., Dauphas N., Luguet A., Pearson D. G., Gallino R. and Zimmermann C. (2009) Nucleosynthetic osmium isotope anomalies in acid leaches of the Murchison meteorite. *Earth Planet. Sci. Lett.* **277**, 334–344.

Savina M. R., Davis A. M., Tripa C. E., Pellin M. J., Clayton R. N., Lewis R. S., Amari S., Gallino R. and Lugaro M. (2003) Barium isotopes in individual presolar silicon carbide grains from the Murchison meteorite. *Geochim. Cosmochim. Acta* **67**, 3201–3214.

Savina M. R., Davis A. M., Tripa C. E., Pellin M. J., Gallino R., Lewis R. S. and Amari S. (2004) Extinct technetium in silicon carbide stardust grains: implications for stellar nucleosynthesis. *Science* **303**, 649–652.

Schönbächler M., Rehkämper M., Fehr M. A., Halliday A. N., Hattendorf B. and Gunther D. (2005) Nucleosynthetic zirconium isotope anomalies in acid leachates of carbonaceous chondrites. *Geochim. Cosmochim. Acta* **69**, 5113–5122.

Shen J. J., Papanastassiou D. A. and Wasserburg G. J. (1996) Precise Re–Os determinations and systematics on iron meteorites. *Geochim. Cosmochim. Acta* **60**, 2887–2900.

Smoliar M.I. (1998) Ru isotopic anomalies in iron meteorites: outlook for the Tc–Ru–Mo chronometers. *Lunar Planet. Sci. Conf. XXIX*. Lunar Planet. Inst., Houston. #1202.

Wasserburg G. J. (1985) Short-lived nuclei in the early solar system. In *Protostars and Planets II* (eds. D. C. Black and M. S. Matthews). University of Arizona Press, Tucson, pp. 703–773.

Wasserburg G. J., Busso M., Gallino R. and Raiteri C. M. (1994) Asymptotic giant branch stars as a source of short-lived radioactive nuclei in the solar nebula. *Ap. J.* **424**, 412–428.

Wasserburg G. J., Busso M. and Gallino R. (1996) Abundances of actinides and short-lived non-actinides in the interstellar medium: diverse supernova sources for the r-process. *Ap. J. Lett.* **466**, L109–L113.

Yin Q.-Z., Jagoutz E. and Wänke H. (1992) Re-search for extinct ^{99}Tc and^{98}Tc in the early solar system. *Meteoritics* **27**, 310.

Yin Q., Jacobsen S. B. and Yamashita K. (2002) Diverse supernova sources of pre-solar material inferred from molybdenum isotopes in meteorites. *Nature* **415**, 881–883.

Yin Q.-Z., Lee C.-T. A. and Ott U. (2006) Signatures of the s-process in presolar silicon carbide grains: Barium through Hafnium. *Ap. J.* **647**, 676–684.

Yokoyama T., Rai V. K., Alexander M. O., Lewis R. S., Carlson R. W., Shirey S. B., Thiemens M. H. and Walker R. J. (2007) Osmium isotope evidence for uniform distribution of s- and r-process components in the early solar system. *Earth Planet. Sci. Lett.* **259**, 567–580.

Associate editor: Sara S. Russell